ARCHIVES OF ELECTRICAL ENGINEERING VOL. 72(1), pp. 157–172 (2023)

DOI 10.24425/aee.2023.143695

New directions in electric arc furnace modeling

DARIUSZ GRABOWSKI ✉, MACIEJ KLIMAS

Faculty of Electrical Engineering, Silesian University of Technology
Akademicka 10 str., 44-100 Gliwice, Poland
e-mail: {✉dariusz.grabowski/maciej.klimas}@polsl.pl

(Received: 10.08.2022, revised: 04.11.2022)

Abstract: This paper presents new directions in the modeling of electric arc furnaces. This work is devoted to an overview of new approaches based on random differential equations, artificial neural networks, chaos theory, and fractional calculus. The foundation of proposed solutions consists of an instantaneous power balance equation related to the electric arc phenomenon. The emphasis is mostly placed on the conclusions that come from a novel interpretation of the equation coefficients.

Key words: artificial neural networks, chaos theory, electric arc furnace, fractional calculus, power balance, stochastic processes

1. Introduction

Various branches of industry have been strongly dependent on steel elements for decades. The range of applications of this robust metal is very wide and has not changed drastically over the years. However, what does change is the idea behind its production, which due to the properties of the metal, requires large amounts of energy. In modern industry, awareness of the limitations related to environmental protection, economic costs, or availability of fossil fuels resulted in increasing focus oriented on the use and improvement of steel production methods such as electric arc furnaces (EAFs). The EAFs have been known to metallurgy for many years, but relatively recently research related to their impact on power quality became very important.

Due to the dynamic, nonlinear and stochastic nature of the electric arc phenomenon occurring in the EAFs, the power supply system can be exposed to, among others, harmonics, voltage sags or swells, and other undesired transients [1]. In order to correctly design and implement power quality improvement systems that mitigate these issues, it is necessary to have an accurate digital or physical model of the EAF [2, 3]. Furthermore, such models can positively influence EAF control systems, resulting in an improvement in their effectiveness [4].

The most widely used and easiest to analyse EAF models are digital ones, most often based on the Cassie, Mayr, hybrid Cassie-Mayr [5] and power balance equations. These, however, are most often used to simulate steady state, which in a real furnace never occurs because of random effects of the electric arc and behavior of the furnace charge. These properties are, sometimes, incorporated into the considered models with the addition of chaotic [6], modulated [7], or stochastic [8] components, mostly directly in the time domain, but such an approach can also be used to represent variations in each harmonic component [9]. Apart from models based on differential equations, models based on an artificial neural network (ANN) are also popular. For example, supported with suitable feature extraction methods, such models are capable of modeling the dynamic $v-i$ characteristic of the EAF without any physical model as support [10].

The aim of this work is to investigate the potential of four different theoretical approaches in the development of more accurate models of the EAF. The proposed directions include random differential equations, artificial neural networks, chaos theory, and fractional calculus. The foundation for the development of each model consists of the instantaneous power balance equation. In the following sections, the measurement data used for model development are presented along with the implementation and comparison of the models taking into account the deterministic and stochastic parts. Additionally, the occurrence of two types of stochastic properties of the EAF is taken into account. The implications of methods required for the comparison of stochastic models are also discussed. This paper is a summary and comparison of previous research made throughout recent years regarding the topic of EAF modeling. The results of comparison allow indication of strengths and weaknesses of each method. Consequently, it leads to selection of the model that will best suit further sharing through direct implementation in transient simulation software. This, in turn, would support analyses related to the design of power systems or power quality improvement systems in real industrial facilities.

2. Electric arc furnace

2.1. Construction and electrical equipment

The main part of the three-phase EAF consists of a chamber in which the furnace charge is placed. The roof of the chamber is equipped with three movable graphite electrodes. The electrodes are electrified, and when they reach a certain height in close proximity to the load, the electric arcs ignite. The heat generated by this phenomenon melts the steel until it reaches the desired physical conditions. The furnace work cycle includes: charging, melting, refining, de-slagging, and tapping stages.

A simplified schematic of the EAF electrical circuit is presented in Fig. 1. It consists of a supply HV/MV transformer (T_1) and an electric arc furnace MV/LV transformer (T_2). Next, X_{LSC} represents short circuit reactance at Bus 1, L_f and R_f represent the inductance and resistance of the feeder connecting the supply transformer and the EAF transformer, L_c and R_c represent the equivalent impedance of the flexible cables, bus conductors, and graphite electrodes. T_1 is a 400/63/33 kV transformer. Then a T_2 63/0.718 kV transformer is connected to the EAF with flexible cables. During measurements conducted on the low voltage side of the furnace transformer, the L_c and R_c parameters can significantly influence the results, so it is necessary to subtract related voltage drops.

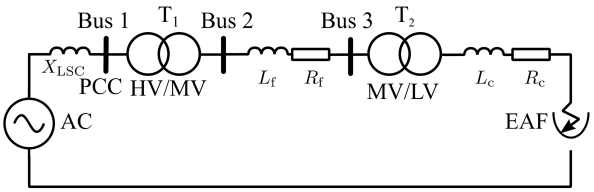

Fig. 1. Simplified diagram of the EAF circuit

2.2. Deterministic model

Although the EAF is most often constructed as a three-phase device, a description of a single-phase current and voltage is sufficient as it can then be extended to three phases. Therefore, we will limit further considerations to the description of a single electric arc phenomenon. The solutions proposed in this paper are based on a nonlinear differential equation originating from an instantaneous power balance of the electric arc. It was introduced by Acha, Semlyen, and Rajakovic [11] and takes the following form:

$$k_1 r^n(t) + k_2 r(t) \frac{\mathrm{d}r(t)}{\mathrm{d}t} = \frac{k_3}{r^{m+2}(t)} i^2(t), \tag{1}$$

where: k_j represents model coefficients ($j = 1, 2, 3$), m and n are the parameters related to an EAF work cycle ($m, n = 0, 1, 2$), $r(t)$ is the arc radius, $i(t)$ is the arc current.

The model is also supplemented by an additional equation that describes the voltage:

$$v(t) = \frac{k_3}{r^{m+2}(t)} i(t). \tag{2}$$

The parameters m and n of (1) are related to a stage in which EAF operates. Most often, their values are assumed to take values of $m = 0$ and $n = 2$, which corresponds to the melting stage. On the other hand, k_j coefficients are related to the proportionality of power accumulated and dissipated through the arc column. Most often, they are assumed constant and their original values were proposed by Ozgun and Abur [12]: $k_1 = 3\,000$, $k_2 = 1$ and $k_3 = 12.5$. The paper focuses specifically on the EAF melting stage, so the parameters m and n are assumed to be constant and equal to 0 and 2, respectively.

The model described by (1) has been approved by the IEEE Task Force on Harmonics Modeling and Simulation as one of the most important arc models [13]. Additionally, it has been implemented, among others, in PSCAD software [14]. However, in the presented form, it is only capable of representing the deterministic properties of the EAF characteristic.

2.3. Stochastic properties of the EAF

As stated in the introduction, the EAF is an example of disturbing load which can cause many different power quality problems. The most challenging aspect of the EAF influence on the power system is that the arc behaves randomly. These stochastic properties are also observable in the measurement data, which is a foundation for the development of the EAF model. Figure 2 presents an exemplary measurement data set consisting of single-phase current and voltage waveforms,

both in long- and short-term perspective. The figure shows the measurement dataset that was a base for the development of the EAF models presented in our previous works, cited appropriately in the following sections.

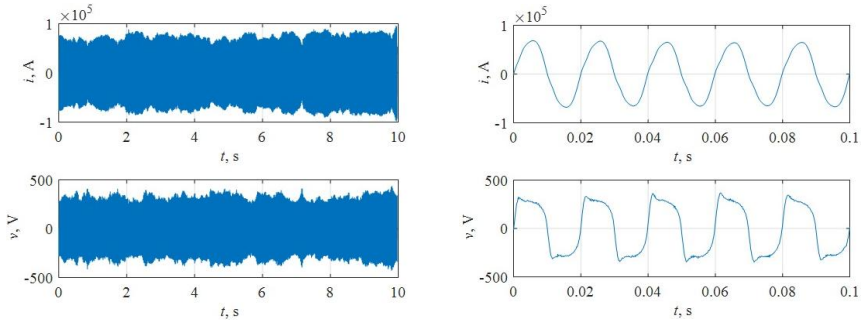

Fig. 2. Measured current and voltage waveform of a single phase of EAF during the melting stage in long- (a) and short-term perspective (b) [15]

As shown, there are two main stochastic properties that are observable in the data. The first one is related to global changes of the characteristic shape, which is also related to variations in the envelope of both measured signals. The second local stochastic behavior is more visible around the peak values of the voltage waveforms. It takes the form of high-frequency ripples, which are only present in the voltage signal.

3. New models of the electric arc furnace

An accurate model of the electric arc phenomenon should incorporate all of its properties, including not only the deterministic part, but also both stochastic properties. The main goal of this paper is to examine the possibilities of developing an arc representation more accurate than that based solely on (1). For this purpose, we have investigated several different theoretical approaches, such as random differential equations (RDEs), artificial neural networks (ANNs), chaos theory, and fractional calculus.

Each approach has its strengths and weaknesses – each has a potential for improving the representation of the electric arc phenomenon, but some are limited to improving the accuracy only in chosen areas, e.g., only in terms of global stochastic properties. In order to organize and provide a clear layout of the contribution of this paper, we have sorted all of the developed models into categories designated by a theoretical basis and the type of property that the model reflects. The summary was introduced in Table 1, which contains the names or abbreviations of the specific methods used for the implementation of each approach. The following subsections provide their description and exemplary.

What is significant is that all of the proposed solutions that incorporate stochastic processes of the EAF rely on a novel interpretation of the existing coefficients of (1). Namely, we propose

Table 1. Summary of EAF models with a breakdown between theoretical approaches and their ability to reflect different EAF properties

Model range		**Model type**					
		ODE	**RDE**	**ANN**		**Chaos theory**	**Fractional calculus**
Deterministic part		Power balance equation	–	Dual MLP		–	HW-based models
Stochastic part	**Global**	–	Stochastic processes identification	M-NARX	LSTM	Chaotic models	
	Local	–		–		–	-

a resignation from the assumption that k_j are constant. Instead, we suggest the assumption that the aforementioned stochastic properties are caused by the variations of those coefficients.

3.1. Random differential equations

The first proposed model is focused on the novel interpretation of the k_j coefficients. The main assumption is that their values are no longer constant, and instead they are responsible for the variations observed in the EAF characteristic. Due to the frequency of those variations, we have also assumed that the k_j coefficients are not continuous but discrete-time processes. Namely, it is assumed that they are constant throughout a frame of a certain length, and then their value changes for the next frame.

The estimation of the k_j values was conducted based on the measurement data but separately and iteratively for each frame. Estimation related to a single frame was performed with a genetic algorithm (GA). The frame-long clipping of the current waveform was taken as input to (1), which, together with (2), allows the calculation of the output voltage. The output voltage was then compared to the clipping of the measured voltage. The GA was applied in order to minimize the root mean square error (RMSE) between both signals to obtain best fitting values of k_j coefficients for each frame. Formally, the optimization problem can be described as follows:

$$\min_{k_1,k_2,k_3} \sqrt{\frac{1}{N}\sum_{i=1}^{N}(v_i - \hat{v}_i)^2}\,, \tag{3}$$

where: v_i is the i-th sample of the measurement voltage, $\hat{v}_i$ is the i-th sample of the simulated voltage, N is the number of samples in the frame.

In this way, three discrete-time stochastic processes K_j, were obtained. In order to ensure proper identification, we have tested different lengths of the frame and starting points of the data division. The analysis suggested that period-long frames are appropriate, and it did not show any significant differences between different starting points. The K_j processes are visualized in Fig. 3. Detailed investigation of properties of the coefficient estimation can be found in our previous papers [15] and [16].

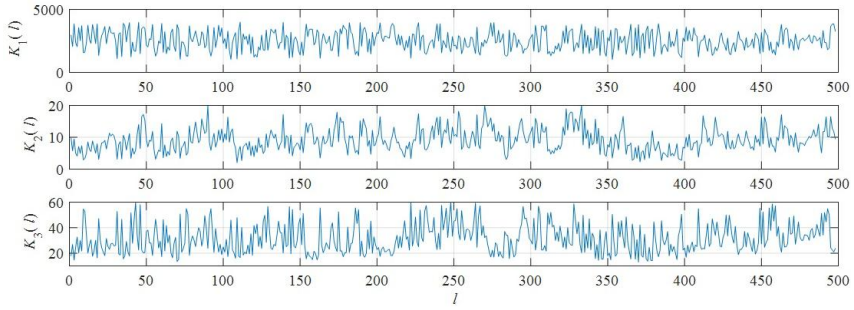

Fig. 3. K_j discrete-time stochastic processes obtained from the measurement data [17]

Due to such an interpretation of the coefficients of (1), the formula actually becomes an RDE:

$$K_1(l)R^2(t) + K_2(l)R(t)\frac{\mathrm{d}R(t)}{\mathrm{d}t} = \frac{K_3(l)}{R^2(t)}I^2(t), \tag{4}$$

where: K_j (l) are coefficients represented by discrete-time stochastic processes ($j = 1, 2, 3$), l is the current frame number, $l = \left[\frac{t}{T_w}\right]$, T_w is the length of a frame, $R(t)$ is the stochastic process representing arc radius, $I(t)$ is the stochastic process representing arc current, $V(t)$ is the stochastic process representing arc voltage:

$$V(t) = \frac{K_3(l)}{R^2(t)}I(t). \tag{5}$$

Such an approach results in a model capable of reflecting the global stochastic behavior of the EAF. However, local stochastic properties are not included. Incorporation of those requires a more detailed description of the voltage ripples observed in the measurement data. Firstly, we have filtered out low-frequency components in order to investigate the ripples only. To do so, we have applied a high-pass filter with cutoff frequency of 600 Hz to the voltage waveform. The obtained signal is presented in Fig. 4.

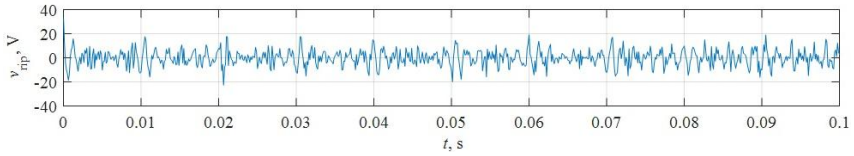

Fig. 4. High-frequency component of the measured voltage waveform – ripples related to local stochasticity [17]

The further analysis consisted of the calculation of autocorrelation (ACF) and partial autocorrelation of the ripple signal, as well as of its first order difference $\Delta v_{\mathrm{rip}} = v_{\mathrm{rip}}(n) - v_{\mathrm{rip}}(n-1)$, $n = 2, 3, 4, \ldots$.

The results presented in Fig. 4 and Fig. 5 suggest that the ripple signal can be directly represented with a stochastic process. An addition of this high-frequency signal to the output waveform obtained with (4) and (5) results in the overall output of the RDE model capable of reflecting not only the deterministic part of the EAF characteristic, but also global and local stochastic changes.

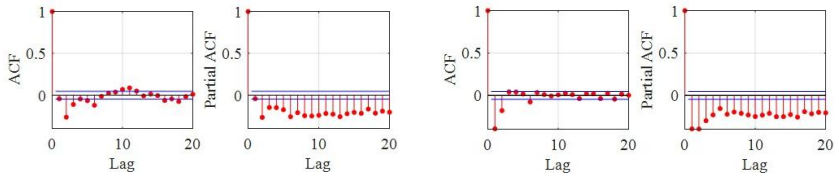

Fig. 5. Autocorrelation and partial autocorrelation of the v_{rip} (a) and Δv_{rip} (b) signals [18]

3.2. Artificial neural networks

The next proposed approach is based on the application of ANNs, which are very popular and widely used tools appropriate for many different purposes. There are a variety of different topologies of ANNs. There are many advanced ANN-based approaches supporting functionality of the EAFs, however, many of them are related to the metallurgical processes or the structural health of the device itself, as shown, e.g., in [19] and [20]. Some of the other existing methods are more similar to ours because they too are focused on modeling of the electrical properties of the EAF. Sometimes various sets of features are taken into account, and the output information differs – some methods model the $v - i$ characteristic directly [21, 22], while others focus, i.e., on power quality measures [23]. Here, for EAF modeling, we have chosen three ANN models, two of which belong to the group of shallow neural networks, while the third belongs to deep learning methods.

The first shallow model comes in two versions, both of which apply a Multilayer Perceptron (MLP) neural network. This universal approximator is designed to be trained to reflect the relation between input and output with minimal error. In this paper, an MLP model was used as a black box model trained directly with current waveform as input and voltage waveform as output. It was intended as a reference point for other solutions. The second version of the MLP model assumed the use of two identical MLP networks (dual MLP model), one reflecting the part of EAF characteristic with rising current and the second for the part with falling current. This allowed us to train the model to properly reflect the hysteresis visible in the characteristic, unlike the first version. However, both versions could not reflect any stochastic properties.

A second shallow model was designed in order to reflect not only static hysteresis of the EAF characteristic but also its dynamic changes. In order to do so, the model described with (1) was transformed into a form where the current was still an input, but the arc conductance was an output. This approach allows separation of a linear dynamic block which we have modeled with a modified nonlinear exogenous model (M-NARX) presented in Fig. 6.

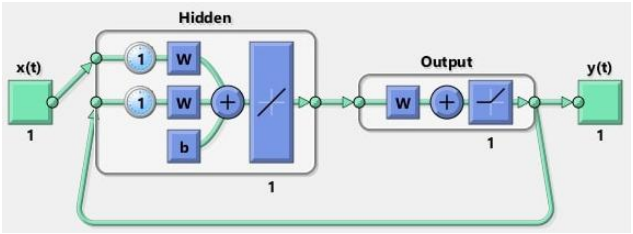

Fig. 6. Topology of the M-NARX model used to simulate arc conductance [24]

The second shallow model has indeed introduced the dynamic properties into the simulated EAF characteristic, but none of the shallow ANNs were able to include the local stochastic part. In order to develop an ANN-based model that was capable of doing so and to test other, modern solutions, we have developed a deep learning model based on long short-term memory (LSTM) cells. An LSTM network consists of multiple LSTM cells that are equipped with gates that allow certain information to be retained throughout its operation. In this way, the LSTM networks are capable of learning and reproducing various properties of long signals.

In our application, four separate LSTM networks were implemented and trained with the stochastic processes obtained by estimating the parameters of (1). The exact datasets used for this purpose are presented in a previous subsection devoted to the RDE model in Fig. 3 and Fig. 4. In this way, the LSTM networks were applied instead of a detailed stochastic process identification procedure in order to learn and replicate appropriate stochastic processes independently. This in turn, once again results in an EAF model which is capable of reflecting both global and local stochastic parts. A more detailed description of the proposed shallow and deep models has been provided in our previous papers [17] and [18].

3.3. Chaos theory

The next proposed approach is based on an application of chaotic systems. Chaotic signals, although deterministic, can behave unpredictably due to their high sensitivity to initial conditions and limited numerical accuracy. Our idea was to incorporate chaotic properties in order to obtain stochastic-like signals which would represent the global stochastic properties of the EAF. A similar approach can be found in [25], where a signal from the Lorenz chaotic system is used to modulate the arc resistance and inductance. Our method differs from this example because it applies a chaotic signal to represent changes of power balance equation coefficients, not the resistance and inductance directly.

Similarly to the model presented in previous subsection, we have proposed a solution to adapt chosen chaotic system to the stochastic processes K_j described in Section 3.1, (shown in Fig. 3). For this purpose, we have selected four different chaotic systems: Lorenz system, a system that describes the Chua circuit, Rössler system, and a four-wing attractor system introduced in [26]. In order to ensure the best match between the generated chaotic signals and stochastic processes K_j, we have conducted an optimization of the selected parameters. In the following, we present this approach on the example of the Lorenz system, which was formulated by E. Lorenz

during his research on thermal convection. It can be described by the following set of differential equations:

$$\begin{cases} \dfrac{\mathrm{d}x}{\mathrm{d}t} = L_1(y - x), \\ \dfrac{\mathrm{d}y}{\mathrm{d}t} = x\,(L_2 - z) - y, \\ \dfrac{\mathrm{d}z}{\mathrm{d}t} = xy - L_3 z, \end{cases} \tag{6}$$

where: L_1 is the coefficient related to the Prandtl number, L_2 is the coefficient related to the Rayleigh number, L_3 is the geometric factor.

The Lorenz system dynamics is often considered for $L_1 = 10$, $L_3 = \dfrac{8}{3}$ and a variable L_2. However, for chaotic behavior, L_2 must be greater than

$$L_2' = \frac{L_1(L_1 + L_3 + 3)}{L_1 - L_3 - 1} = 24.74.$$

In order to fit the selected variable x to the K_j process, we have conducted an optimization of the L_2 value and of a sampling frequency of signal x, denoted by f_s. Both parameters should be fitted so as to obtain stochastic-like signals which correspond to the target not only with the distribution of their values but also their autocorrelation. Therefore, we have proposed two goal functions which apply the Cramér-von Mises distance between the simulated and target histograms as well as their autocorrelation functions. The functions are as follows:

$$\begin{aligned} f_1(\cdot) &= \sum_{p=1}^{N} \left(h_p^{\text{meas}} - h_p^{\text{chaotic}} \right)^2, \\ f_2(\cdot) &= \sum_{p=1}^{M} \left(ACF_p^{\text{meas}} - ACF_p^{\text{chaotic}} \right)^2, \end{aligned} \tag{7}$$

where: h_p is the p-th histogram bar (from measurement or simulated data), N is the number of the histogram bars, ACF_p is the autocorrelation value for the p-th lag, M is the number of the considered lags.

The same procedure as described above was repeated for remaining chaotic systems, where again sampling frequency f_s and one selected parameter was fitted. The overall combined model had the best precision for the representation of K_1 and K_3 with the Lorenz system and K_2 with the four-wing attractor system. The details of this approach have been presented in our previous paper [27].

3.4. Fractional calculus

Apart from the aforementioned solutions oriented on incorporating of the stochastic part into the EAF model, we have also developed a solution for improving the deterministic part described by the power balance equation. Due to the fact that the electric arc is a complex phenomenon, we have proposed an extension of the ODE model to a more general form which includes non-integer

order of differentiation. Such a model, based on the fractional calculus, would be suitable for more states than a classic one.

The idea behind this approach can be well explained with the support of a visual representation of (1). Figure 7 presents a block diagram of the basic power balance model [28]. This model is a Hammerstein–Wiener (HW) model, which is characterized by the separation of two nonlinear static blocks from one linear dynamic block in the middle. In order to incorporate the fractional calculus into this model, we have replaced the integration block in the linear part of the model with a more general block representing the integro-differential operator. Such an operator is described as [29]:

$$ {}_aD_t^{\alpha} = \begin{cases} \dfrac{\mathrm{d}^{\alpha}}{\mathrm{d}t^{\alpha}} & : \quad \alpha > 0, \\ 1 & : \quad \alpha = 0, \\ \displaystyle\int_a^t (\mathrm{d}t)^{\alpha} & : \quad \alpha < 0. \end{cases} \tag{8} $$

where: a and t are the bounds of the operation and α is an order of the fractional operator, $\alpha \in R$.

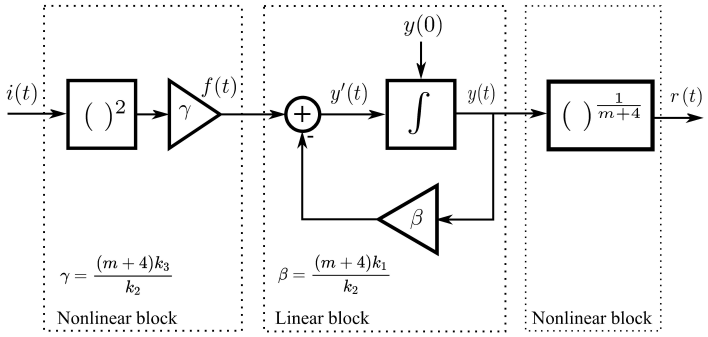

Fig. 7. Block diagram of the power balance equation of the electric arc

For numerical calculations, the Grünwald-Letnikov (GL) implementation of operator (8) is often used. It can be described as follows:

$$ {}_aD_t^{\alpha} y(t) = \lim_{T_s \to 0} \frac{1}{T_s^{\alpha}} \sum_{j=0}^{\left[\frac{t-a}{T_s}\right]} (-1)^j \binom{\alpha}{j} y\left(t - jT_s\right), \tag{9} $$

where T_s is the sampling period.

In order to estimate α fitting the measurement data in the best possible way, we have again conducted the estimation process as described in Section 3.1 but with extension to two cases that include the fractional version of the power balance equation: one with $\alpha \neq 1$ throughout all frames and one with variable $\alpha = \mathrm{var}$. The variable α case assumes that, similar to the k_j coefficients, its value remains constant for each period-long frame and then for the next frame a new value is fitted independently. This way, we have obtained information regarding the quality of representation of the arc characteristic extended to either constant or variable, non-integer order

of differentiation. The results derived from this approach indicate that incorporation of a fractional order to the equation allows better reflection of the EAF waveform shape. The identification of stochastic processes governing the fractional order model is yet to be conducted in the nearest future. Therefore, the fractional model, capable of generating appropriate stochastic realizations by itself will be the subject of next publications.

4. Exemplary results

The procedures described in the previous section constitute the theoretical background for the development of EAF models. Based on the results of data-driven optimization algorithms and stochastic process identification, we have implemented the models in Matlab software. In order to present and compare their capabilities, we have applied an exemplary clipping of the measurement current waveform as the input and computed the output voltage. The applied input current was the same for all models. The output waveform was then compared to the respective clipping of the measurement voltage. The waveforms obtained for each implemented model were presented in Fig. 8. It is worth stressing that every model that includes the stochastic part does not exactly mimic the measurement waveform. The voltage signals generated by them are only single exemplary realizations obtained by means of stochastic processes. Therefore, the discrepancies between the presented realizations are not related to the errors in modeling but rather to differences between two independent realizations of the stochastic processes. In the case of models reflecting only the deterministic part, such an exact comparison is, in turn, desirable.

In order to bring more details for comparison between the models, we have also introduced a statistical measure based on the RMS error of averaged voltage waveforms either from the measurement or simulation data. Each sample of the averaged voltage has been calculated as a mean value of corresponding points taken from the consecutive periods throughout all 10 s long dataset. Additionally, we have calculated a standard deviation for each of those points. Similarly to the approach presented in our previous work [18], we have calculated two errors, one is the RMS of the difference between the averaged model output and averaged measurement voltage. The second is the RMS value of the difference between the standard deviations computed from the averaged model output and the averaged measurement voltage. Both results have been divided by the RMS of the averaged voltage and expressed in percentages:

$$\varepsilon_{\mu v} = \sqrt{\frac{\int_0^{T_0} (v_{\mathrm{AVG}}(t) - \hat{v}_{\mathrm{AVG}}(t))^2 \,\mathrm{d}t}{\int_0^{T_0} (v_{\mathrm{AVG}}(t))^2 \,\mathrm{d}t}} \cdot 100\% = \frac{|\Delta V_{\mathrm{AVG}}|}{|V_{\mathrm{AVG}}|} \cdot 100\%, \tag{10}$$

$$\varepsilon_{\sigma v} = \sqrt{\frac{\int_0^{T_0} (\sigma_v(t) - \hat{\sigma}_v(t))^2 \,\mathrm{d}t}{\int_0^{T_0} (v_{\mathrm{AVG}}(t))^2 \,\mathrm{d}t}} \cdot 100\% = \frac{|\Delta \sigma_v|}{|V_{\mathrm{AVG}}|} \cdot 100\%\,. \tag{11}$$

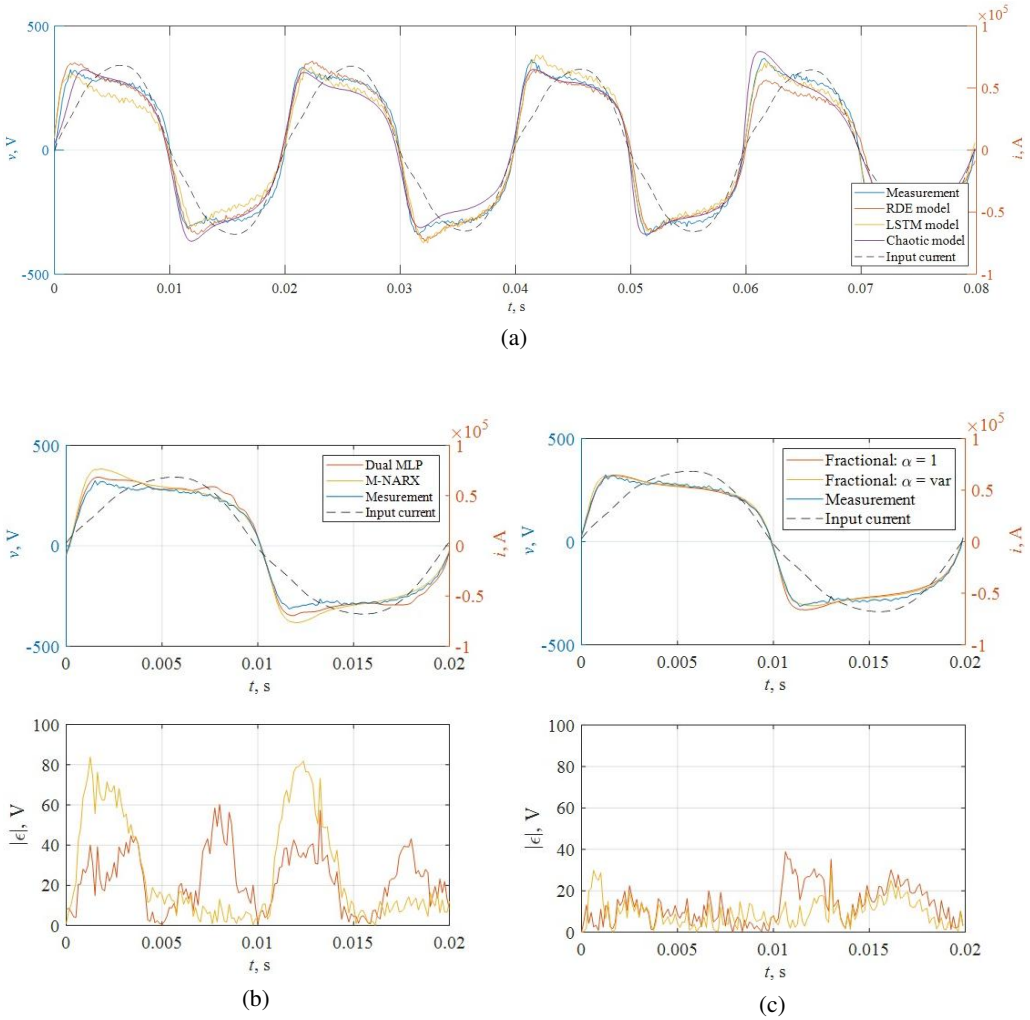

Fig. 8. Comparison between measurement voltage and the simulated voltages obtained by RDE, LSTM and chaotic models (a); shallow ANN models (b) and fractional models (c)

What is different from the results from the cited paper is that here we have applied longer datasets for the error calculation in order to investigate the performance of proposed models throughout richer input data. Therefore, the models have been subjected to larger changes of the shape and amplitude of the input signals. An exemplary visual comparison of the data used for error calculation is presented in Fig. 9, while exact error measures are presented in Table 2.

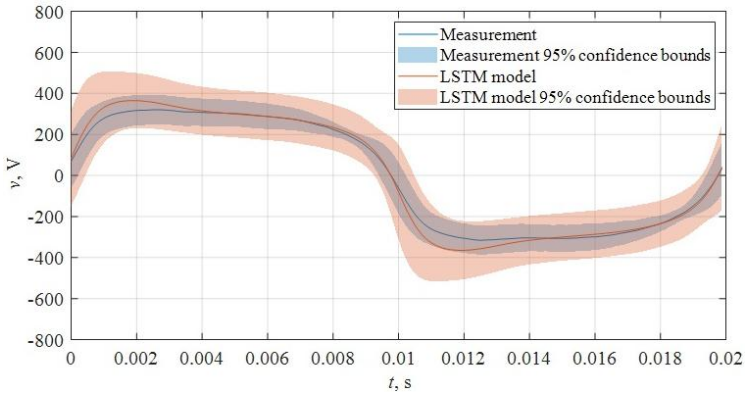

Fig. 9. Comparison between averaged measurement voltage and averaged LSTM model output, both with 95% confidence bounds calculated based on standard deviation of the samples

Table 2. Summary of EAF model performance using measure described with (10) and (11)

	RDE	**Chaotic**	**ANN**		
			Dual MLP	**M-NARX**	**LSTM**
Averaged voltage root mean square error, $\varepsilon_{\mu v}$	16.4%	8.5%	14.2%	13.9%	10.9%
Standard deviation root mean square error, $\varepsilon_{\sigma v}$	27.2%	16.8%	12.5%	8.5%	13.2%

5. Conclusions

This article presents the development of some new EAF models using four different theoretical approaches, i.e. random differential equations, artificial neural networks, chaos theory, and fractional calculus. We have presented the potential of each new direction in modeling of both the deterministic and stochastic components. We have implemented several models incorporating deterministic and stochastic properties and compared their outputs. Each proposed solution effectively satisfies the appropriate initial assumptions about its performance. Moreover, every model is based on the measurement data obtained from a real furnace and therefore accurately reflects phenomena observable in industrial power systems.

Due to the random nature of the EAF, a detailed and quantitative comparison of stochastic models requires suitable statistical methods. It is worth stressing that in the case of the models which output only a single realization of a stochastic process, their output cannot be directly compared with the target signal using classic error measures such as, for example, RMSE. Instead, more complex statistical measures shall be applied. We have introduced such a measure based on averaged voltage waveforms. The quantitative comparison indicated that among the proposed models, the chaotic model is characterized by the lowest error related to the general averaged shape of the waveform, whereas the M-NARX model has the lowest error in terms of

the standard deviation. The relatively large error obtained for RDE models mainly connected with the simplifying assumption that states the lack of correlation between the k coefficients described with the stochastic processes. The advantages of this model in terms of simplicity of implementation and coverage of the autocorrelation features of the coefficients prevent one from arguing that it is not useful compared to others before further investigation. Such research is planned in the future.

Acknowledgements

This work was supported in part by the government funds for science for years 2019–2023 as part of the "Diamond Grant" program, and in part by the European Union Through the European Social Fund under Grant POWR.03.05.00-00-Z305.

References

[1] Jebaraj B.S. *et al*., *Power Quality Enhancement in Electric Arc Furnace Using Matrix Converter and Static VAR Compensator*, Electronics, vol. 10, no. 9 (2021), DOI: 10.3390/electronics10091125.

[2] Łukasik Z., Olczykowski Z., *Estimating the Impact of Arc Furnaces on the Quality of Power in Supply Systems*, Energies, vol. 13, no. 6 (2020), DOI: 10.3390/en13061462.

[3] Wciślik M., Strząbała P., *Physical model of power circuit of three-phase electric arc furnace*, Przegląd Elektrotechniczny, vol. 4, pp. 103–106 (2018), DOI: 10.15199/48.2018.04.26.

[4] Nikolaev A.A., Tulupov P.G., Savinov D.A., *Mathematical model of electrode positioning hydraulic drive of electric arc steel-making furnace taking into account stochastic disturbances of arcs*, Proceedings of 2017 International Conference on Industrial Engineering, Applications and Manufacturing (ICIEAM), St. Petersburg, Russia, pp. 1–6 (2017), DOI: 10.1109/ICIEAM.2017.8076205.

[5] Sawicki A., *Electric arc models with non-zero residual conductance and with increased energy dissipation*, Archives of Electrical Engineering, vol. 70, no. 4, pp. 819–834 (2021), DOI: 10.24425/aee.2021.138263.

[6] Lu T., Sun Y., Shen P., An P., Diao S., *Study on Time-varying Resistance Model of Arc Furnace Based on Arc Length Modulation and PSO Algorithm*, Proceedings of 2020 IEEE/IAS Industrial and Commercial Power System Asia (I&CPS Asia), Weihai, China, pp. 513–518 (2020), DOI: 10.1109/ICPSAsia48933.2020.9208494.

[7] Teklić A.T., Filipović-Grčić B., Pavić I., *Modelling of three-phase electric arc furnace for estimation of voltage flicker in power transmission network*, Electric Power Systems Research, vol. 146, pp. 218–227 (2017), DOI: 10.1016/j.epsr.2017.01.037.

[8] Mousavi Agah S.M., Hosseinian S.H., Abyaneh H.A., Moaddabi N., *Parameter Identification of Arc Furnace Based on Stochastic Nature of Arc Length Using Two-Step Optimization Technique*, IEEE Transactions on Power Delivery, vol. 25, no. 4, pp. 2859–2867 (2010), DOI: 10.1109/TPWRD.2010.2044812.

[9] Samet H., Sadeghi R., Ghanbari T., *Time-varying frequency model for electric arc furnaces*, IET Generation, Transmission & Distribution, vol. 16, no. 6, pp. 1122–1138 (2022), DOI: 10.1049/gtd2.12355.

[10] Farzanehdehkordi M., Ghaffaripour S., Tirdad K., Dela Cruz A., Sadeghian A., *A wavelet feature-based neural network approach to estimate electrical arc characteristics*, Electric Power Systems Research, vol. 208, p. 107893 (2022), DOI: 10.1016/j.epsr.2022.107893.

[11] Acha E., Semlyen A., Rajakovic N., *A harmonic domain computational package for nonlinear problems and its application to electric arcs*, IEEE Transactions on Power Delivery, vol. 5, no. 3, pp. 1390–1397 (1990), DOI: 10.1109/61.57981.

[12] Ozgun O., Abur A., *Development of an arc furnace model for power quality studies*, Proceedings of 1999 IEEE Power Engineering Society Summer Meeting, Conference Proceedings (Cat. No. 99CH36364), Edmonton, Canada, vol. 1, pp. 507–511 (1999), DOI: 10.1109/PESS.1999.784402.

[13] Chang G. *et al.*, *Modeling devices with nonlinear Voltage-current Characteristics for harmonic studies*, IEEE Transactions on Power Delivery, vol. 19, no. 4, pp. 1802–1811 (2004), DOI: 10.1109/TPWRD.2004.835429.

[14] Ortega-Calderon J.E., *Modelling and analysis of electric arc loads using harmonic domain techniques*, PhD Thesis, Department of Electronics and Electrical Engineering, University of Glasgow, Glasgow (2008).

[15] Klimas M., Grabowski D., *Identification of nonstationary parameters of electric arc furnace model using Monte Carlo approach*, Proceedings of 2020 Progress in Applied Electrical Engineering (PAEE), Kościelisko, Poland, pp. 1–6 (2020), DOI: 10.1109/PAEE50669.2020.9158732.

[16] Dietz M., Grabowski D., Klimas M., Starkloff H.-J., *Estimation and analysis of the electric arc furnace model coefficients*, IEEE Transactions on Power Delivery, pp. 1–1 (2022), DOI: 10.1109/TPWRD.2022.3163815.

[17] Klimas M., Grabowski D., *Application of Long Short-Term Memory Neural Networks for Electric Arc Furnace Modelling*, Proceedings of Intelligent Data Engineering and Automated Learning – IDEAL 2021, Manchester, UK, pp. 166–175 (2021), DOI: 10.1007/978-3-030-91608-4.

[18] Klimas M., Grabowski D., *Application of Shallow Neural Networks in Electric Arc Furnace Modeling*, IEEE Transactions on Industry Applications, vol. 58, no. 5, pp. 6814–6823 (2022), DOI: 10.1109/TIA.2022.3180004.

[19] Li C., Mao Z., *Generative adversarial network–based real-time temperature prediction model for heating stage of electric arc furnace*, Transactions of the Institute of Measurement and Control, vol. 44, no. 8, pp. 1669–1684 (2022), DOI: 10.1177/01423312211052213.

[20] Godoy-Rojas D.F. *et al.*, *Attention-Based Deep Recurrent Neural Network to Forecast the Temperature Behavior of an Electric Arc Furnace Side-Wall*, Sensors, vol. 22, no. 4 (2022), DOI: 10.3390/s22041418.

[21] Golestani S., Samet H., *Polynomial-dynamic electric arc furnace model combined with ANN*, International Transactions on Electrical Energy Systems, vol. 28, no. 7, p. 2561 (2018), DOI: 10.1002/etep.2561.

[22] Ghiormez L., Panoiu M., Panoiu C., Tirian O., *Time series prediction in the case of nonlinear loads by using ADALINE and NAR neural networks*, IOP Conf. Ser.: Mater. Sci. Eng., vol. 294, no. 1, p. 12–26 (2018), DOI: 10.1088/1757-899X/294/1/012026.

[23] Panoiu M., Panoiu C., Ghiormez L., *Neuro-fuzzy modeling and prediction of current total harmonic distortion for high power nonlinear loads*, Proceedings of 2018 Innovations in Intelligent Systems and Applications (INISTA), pp. 1–7 (2018), DOI: 10.1109/INISTA.2018.8466290.

[24] MATLAB, *version 7.10.0 (R2019b)*, Natick, Massachusetts: The MathWorks Inc. (2019).

[25] Jang G., Wang W., Heydt G.T., Venkata S.S., Lee B., *Development of Enhanced Electric Arc Furnace Models for Transient Analysis*, Electric Power Components and Systems, vol. 29, no. 11, pp. 1060–1073 (2001), DOI: 10.1080/153250001753239257.

[26] Qi G. *et al.*, *A four-wing chaotic attractor generated from a new 3-D quadratic autonomous system*, Chaos, Solitons & Fractals, vol. 38, no. 3, pp. 705–721 (2008), DOI: 10.1016/j.chaos.2007.01.029.

[27] Klimas M., Grabowski D., *Application of the deterministic chaos in AC electric arc furnace modeling*, Proceedings of 2022 IEEE International Conference on Environment and Electrical Engineering and 2022 IEEE Industrial and Commercial Power Systems Europe (EEEIC/I&CPS Europe), pp. 1–6 (2022), DOI: 10.1109/EEEIC/ICPSEurope54979.2022.9854594.

[28] Grabowski D., *Selected Applications of Stochastic Approach in Circuit Theory*, Publishing House of the Silesian University of Technology (2015).

[29] Gulgowski J., Stefański T.P., Trofimowicz D., *On applications of elements modelled by fractional derivatives in circuit theory*, Energies, vol. 13, no. 21, 5768 (2020), DOI: 10.3390/en13215768.